SCIENTIFIC REPORTS

OPEN

SUBJECT AREAS:
MECHANICAL PROPERTIES
PHASE TRANSITIONS AND CRITICAL PHENOMENA
NANOPARTICLES
STRUCTURAL PROPERTIES

Received
18 June 2013

Accepted
6 March 2014

Published
24 March 2014

Correspondence and requests for materials should be addressed to D.W.H. (duanweihe@scu.edu.cn)

Unusual Compression Behavior of Nanocrystalline CeO_2

Qiming Wang[1], Duanwei He[1,2], Fang Peng[1], Li Lei[1], Pingping Liu[1], Shuai Yin[1], Pei Wang[1], Chao Xu[1] & Jing Liu[3]

[1]Institute of Atomic and Molecular Physics, Sichuan University, Chengdu 610065, China, [2]Institute of Fluid Physics and National Key Laboratory of Shockwave and Detonation Physics, China Academy of Engineering Physics, Mianyang 621900, China, [3]Institute of High Energy Physics, Chinese Academy of Sciences, Beijing 100049, China.

The x-ray diffraction study of 12 nm CeO_2 was carried out up to ~40 GPa using an angle dispersive synchrotron-radiation in a diamond-anvil cell with different pressure transmitting medium (PTM) (4 : 1 methanol: ethanol mixture, silicone oil and none) at room temperature. While the cubic fluorite-type structure CeO_2 was retained to the highest pressure, there is progressive broadening and intensity reduction of the reflections with increasing pressure. At pressures above 12 GPa, an unusual change in the compression curve was detected in all experiments. Significantly, apparent negative volume compressibility was observed at P = 18–27 GPa with silicone oil as PTM, however it was not detected in other circumstances. The expansion of the unit cell volume of cubic CeO_2 was about 1% at pressures of 15–27 GPa. To explain this abnormal phenomenon, a dual structure model (hard amorphous shell and relatively soft crystalline core) has been proposed.

Nano materials attract much attention not only for their unique enhanced properties, which are different from those of the bulk materials, but also for their fundamental scientific and technological applications. Series of interesting phenomena and novel properties have been revealed when nanosized materials were investigated under high pressures. As an important material in many technological applications including gate for metal-oxide semiconductor devices, ultraviolet (UV) blockers, solar cell, catalysts, and solid oxide fuel cells, the rare earth oxide CeO_2, with a cubic fluorite structure, is considered to be important in the high P-T processing of advanced engineering materials[1–4]. Due to its promising technological applications, numerous investigations have been reported on the structure stabilities and compressibility of different sized CeO_2 under high pressure[5–13]. It is reported that the phase transformation pressure of nanosized CeO_2 decreased compared to that of bulk counterpart[8,9], whereas other studies hinted that nano-CeO_2 remains stable to much higher pressures than the bulk[7,10,11,14]. Moreover, an anomalous compressive behavior of CeO_2 nanocubes, which is due to the strengthening of the surface Ce-O bonds, was observed by Ge *et al.*[5] Therefore, series of interesting phenomena and novel properties have attracted much interest, and continuous high pressure investigations are conducting to reveal the details of the behavior of nano-CeO_2.

In this work, we have carried out three high pressure angle-dispersive x-ray diffraction (ADXD) studies to investigate the structure stabilities and compressibility for 12 nm nanocrystalline (nc) CeO_2 with two different and without pressure transmitting medium (PTM). We found that at pressures above 12 GPa, an unusual change in the compression curve was detected in each experiment. Significantly, in the pressure range of 18–27 GPa, suspected negative volume compressibility (NVC) was observed with silicone oil as PTM, however it was not detected in experiment with mixture of methanol-ethanol (M-E) (4 : 1 by volume) as PTM or without PTM. High-pressure *in situ* x-ray diffraction experiments showed that the expansion of the unit cell volume of cubic CeO_2 was about 1% at pressures of 18–27 GPa. Based on previous high pressure works, a dual structure model (hard amorphous shell and relatively soft crystalline core) has been proposed. This unusual NVC phenomenon is not really a characteristic for nc CeO_2 itself, but a false appearance induced by the formation and thickens of a stiff shell in nanograin under compression with silicone oil as PTM.

Results

Figure 1 displays angle dispersive x-ray diffraction spectra taken at pressure for the 12 nm CeO_2 with silicone oil as PTM. The patterns for other two experiments are similar with Fig. 1 (shown in Fig. S1). While the cubic fluorite-type structure was retained to the highest pressure, there is progressive broadening and intensity reduc-

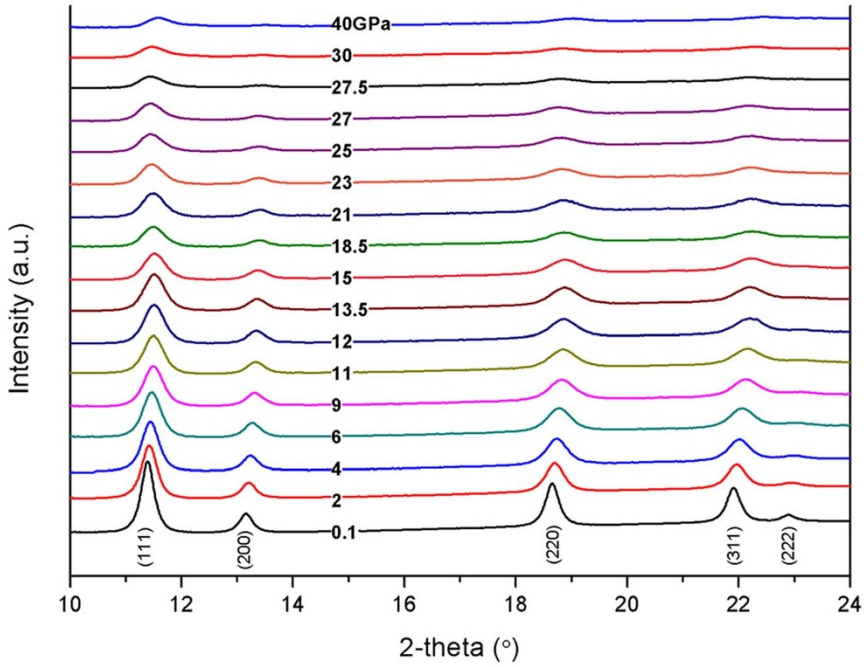

Figure 1 | Integrated *in situ* XRD spectra at various pressures under compression up to 40 GPa with silicone oil as PTM.

tion of the reflections due to increasing strain inhomogeneity and microstrains with increasing pressure. Differences in the elastic properties of nanoparticle interiors and their grain-boundary regions, particle aggregation, and increased nonhydrostaticity due to unavoidable solidification of liquid pressure media likely account for local strain inhomogeneity, but the peak positions used to determine lattice parameters, which contain the information of macrostrain in the elastic deformation, are not affected[15]. Therefore, full XRD spectrum fitting was carried out to obtain the pressure-dependent variations in relative *d*-spacing (d/d_0) as shown in Fig. 2. Upon initial compression, a consistent shift of angle dispersive x-ray diffraction lines to smaller *d*-spacings indicates tighter packing of the atoms with compression. When the pressure increases to 15 GPa, there are clearly unusual stiffness changes in the shift of peak positions as a function of pressure with M-E (4 : 1) or silicone oil as PTM or without PTM. More significantly, obvious shifts toward large *d*-spacings are observed for all diffraction lines as compared to those at 18.5 GPa under compression with silicone oil as PTM. This tendency continues with further compression, and a progressive peak broadening and intensity reduction are accompanied. At pressures beyond 27 GPa, the weak and broad Bragg reflections of the cubic structure start to shift normally to smaller *d*-scale. Above 39 GPa, both with silicone oil as PTM and without PTM, a weak new peak of the high-pressure phase (α-$PbCl_2$-type) was faintly visible as shown in Fig. 3, indicating that the cubic fluorite-type structured nc-CeO_2 begins to transform to the high-pressure phase (α-$PbCl_2$-type).

Table 1 summarizes the main experimental results of high-pressure studies of CeO_2. The differences in the transition pressures at which the structural transitions occur may depend on the nature of the starting materials and the experimental conditions. Considering the detection methods of the determination of the grain size, this work along with a reanalysis of previous studies on nc CeO_2[5–7,10,11,14,16] allow us to reach consistency among several studies of the size dependence of the phase transitions, that is the nanocrystals exhibit elevated phase transition pressures as compared to bulk materials[6,14,17]. This may due to the initial peak broadenings of nanosized starting material and progressive broadening and intensity reduction of the reflections which result from the increasing pressure.

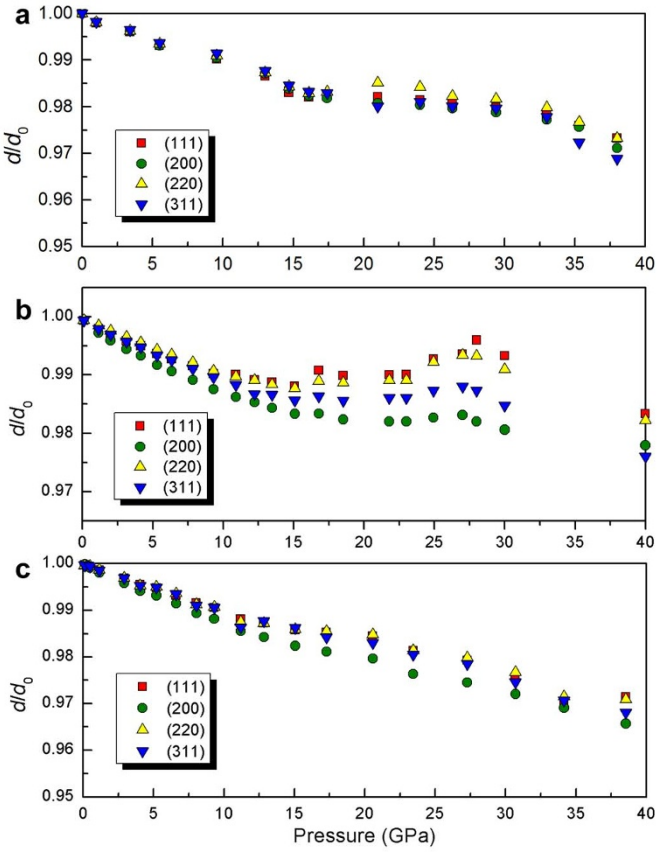

Figure 2 | Variation of relative *d*-spacing (d/d_0) for 12 nm CeO_2 for different Bragg reflections as a function of pressure. (a) with methanol: ethanol mixture (4 : 1) as PTM. (b) with silicone oil as PTM. (c) Nonhydrostatic compression.

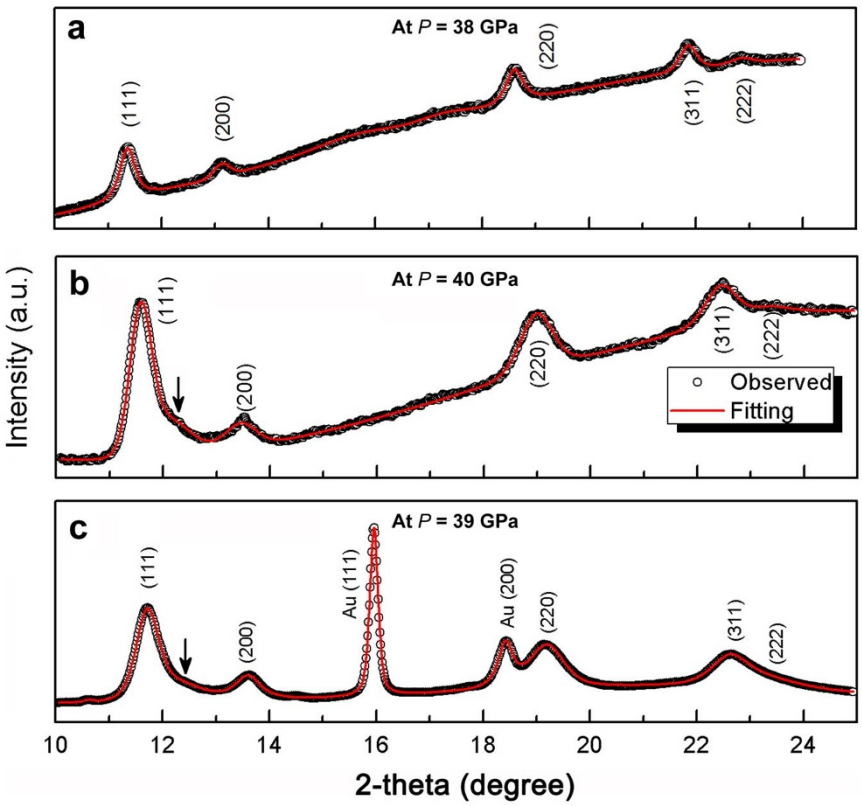

Figure 3 | X-ray diffraction of nano-CeO_2 at the highest pressure under compression with methanol: ethanol mixture (4 : 1) (a) or silicone oil as PTM (b) and without PTM (c). The downward arrow (↓) represents the appearance of the most intense peak of the high pressure CeO_2 phase.

Therefore the weak peaks of the high-pressure phase can be identified at higher pressure compared to that for the bulk counterpart.

Figure 4 displays the variations of refined unit cell parameters for CeO_2 to 40 GPa under compression. Also shown in the figure are data on previous works. At lower pressures ($P < 12$ GPa), the compressibilities of nano-CeO_2 samples are similar to bulk-CeO_2. However, abrupt changes in the compression curves were observed in all data for the nanosized samples at $P > 12$ GPa as shown in Fig. 4. Here we discuss the unusual compressibilities of nano-CeO_2 in two parts, before and after 15 GPa. The pressure-volume (P-V) data for cubic fluorite-type CeO_2 at $P < 15$ GPa was fitted by using a second-order Birch-Murnaghan EOS (BM-EOS)[18] to more easily compare with previous studies (Table 2). Our measured second-order BM-EOS for 12 nm CeO_2 gives a bulk modulus $B_0 = 282(5)$ GPa with $V_0 = 158.64$ (0.15) Å^3 under compression with silicone oil as PTM; whereas for nonhydrostatic condition, we obtain a slight higher value $B_0 = 289$ (13) GPa. It is found that the bulk modulus increases as the particle size decreases to ~10 nm and then decreases in particles less than ~10 nm (Table 2, Fig. S2). Above 15 GPa, clear stiffness changes in the compression curves were observed in all data

Table 1 | Summary of the main results of high-pressure studies of CeO_2[a]

Grain size	DM[b]	Phase Transition		Maximum Pressure (GPa)	Pressure standard	PTM	Method	Reference
		Beginning	Ending					
4.7 nm	TEM	--	--	28	Ruby	16 : 3 : 1	ADXD	5
5.6 nm	TEM	--	--	28		methanol : ethanol : water		
5 nm	TEM	--	--	34	Ruby	4 : 1 methanol : ethanol	Raman	11
10 nm	--	--	--	38	Pt	None	EDXD	10
12 nm	TEM	--	--	51	Ruby	4 : 1 methanol : ethanol	ADXD	14
12 nm	TEM/XRD	40	--	40	Ruby	Silicone oil	ADXD	This study
12 nm	TEM/XRD	39	--	39	Au	None	ADXD	This study
12 nm	TEM/XRD	--	--	38	Ruby	4 : 1 methanol : ethanol	ADXD	This study
36 nm	XRD	34.7	--	35	Ruby	4 : 1 methanol : ethanol	Raman	7
150 nm	TEM	35	>55	55	Ruby	4 : 1 methanol : ethanol	Raman	16
Bulk	--	31.5(1.0)	38	70	Ruby	--	EDXD	6
5 μm	--	27	--	27	Ruby	None	ADXD	12
12 nm	--	26.5(2)	--	36	Ruby	CsCl	Raman	8
12 nm	--	26.5(2)	--	36	Ruby	None		
9-15 nm	--	22.3	--	38.6	Pt	None	EDXD	9

[a]For values not given, - -is shown.
[b]Detection method.

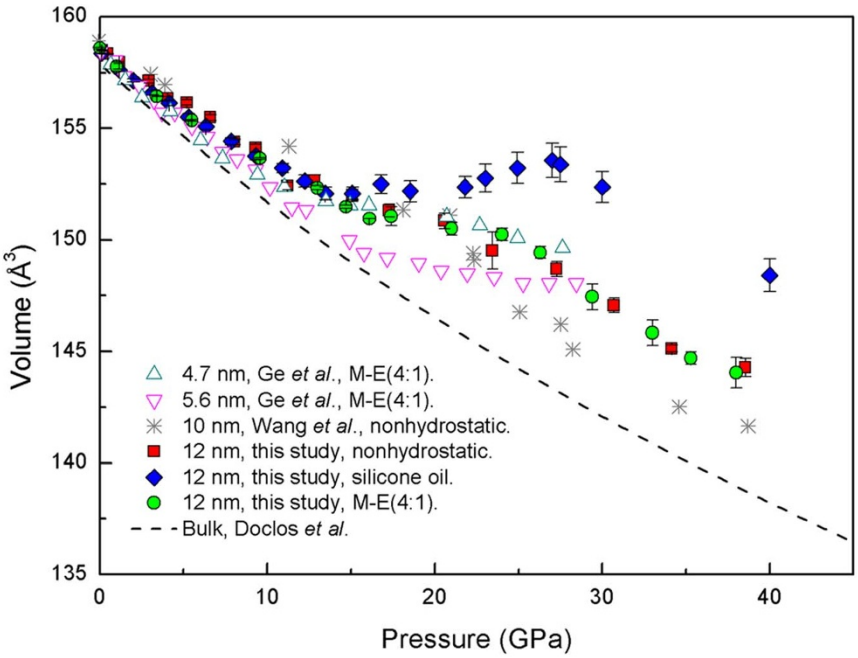

Figure 4 | The pressure-dependent variations of the unit cell volume for CeO_2. Open triangle: 4.7 nm data from Ref. 5; inverted triangle: 5.6 nm data from Ref. 5; star: 10 nm data from Ref. 10; squares (red): 12 nm CeO_2 of this study without PTM; diamonds (blue): 12 nm CeO_2 of this study with silicone oil as PTM; circle (green): 12 nm CeO_2 of this study with M-E (4 : 1) as PTM; dash line (black): bulk data from Ref. 6.

for the nanosized samples at $P > 12$ GPa as shown in Fig. 4. Remarkably, negative volume compressibility was observed for 12 nm CeO_2 at $P = 21.8$–27 GPa with silicone oil as PTM in this study. And the unit cell volume of the cubic CeO_2 was expanded for nearly 1% at pressures of 15.8–27 GPa. With further compression to a critical pressure of about 27 GPa, normal volume contraction recovered, and the unit cell volume started to decrease.

It is thermodynamically impossible for a closed system to have a negative volumetric compressibility[19]. Therefore findings about this phenomenon were disconfirmed as a result of an uptake of additional interstitial molecules[20,21], e.g., hydration[22] or the intercalation of a component of the pressure transmitting medium[19]. However, in this study, the unusual compression phenomenon is not a result of an uptake of the silicone oil for the NVC phenomenon did not happened for bulk-CeO_2 using the same DAC techniques as illustrated in the supplementary materials (Fig. S3). Since the NVC phenomenon was not observed during nonhydrostatic compression up to 39 GPa, we believe that the nonhydrostaticity is not responsible for the formation of the NVC phenomenon. The overall results together with previous works indicate that the NVC phenomenon observed in this study is related with PTM used and the average grain size of the starting material.

Discussion

Surface atoms are different from those of atoms located inside the crystallites for they have fewer interatomic bonds than those in the bulk[23]. Due to the high surface to volume ratio, a nanocrystal cannot be represented uniquely by a unit cell. And the properties of nanocrystalline depend critically on the properties of internal interfaces such as grain boundaries and interphase boundaries[24]. It is reasonable to interpreted a nanograin as a two-phase system[25,26] where a structurally crystalline core is surrounded by a surface disordered (low density amorphous, LDA) shell at room temperature and pressure. Based on the main experimental and theoretical results as below:

(i) First-principles electronic calculations reported by Ge *et al.* show that the increased bulk modulus of the nanocrystal is due to the strengthening of the surface Ce-O bonds resulting in a much larger shear modulus than in the bulk and consequently hardening the shell surface. In other words, results suggested that the shorter and stronger Ce-O bonds are near the surface of the nanocrystal forming a hard shell which is harder to compress[5]. Here we consider the harden shell surface with shorter an stronger Ce-O, which is different from the initially LDA, as high density amorphous (HDA);

Table 2 | Bulk modulus of CeO_2 with a series of particle sizes[a]

Grain size	Pressure range (GPa)	B_0 (GPa)	B_0'	V_0 (Å^3)	EOS-type	PTM	Ref
4.7 nm	0–11	248(5)	4	--	BM	16 : 3 : 1 methanol : ethanol : water	5
5.6 nm	0–12	245(3)	4	--	BM		5
10 nm	0–18	328(12)	4	159.18	BM	None	10
12 nm	0–13	289(13)	4	158.64(15)	BM	None	This study
12 nm	0–13	282(5)	4	158.64(15)	BM	Silicone oil	
12 nm	0–16	287(5)	4	158.64(15)	BM	4 : 1 methanol : ethanol	
150 nm	0–45	260(10)	4	159.04(1)	BM	4 : 1 methanol : ethanol	16
5 μm	0–27	235(18)	3.67	158.44	Vinet	None	12
Bulk	0–37	230(10)	4	157.99	BM	--	6

[a]For values not given, - -is shown. For reference 5, we compute the EOS from the given P-V/V_0 data.

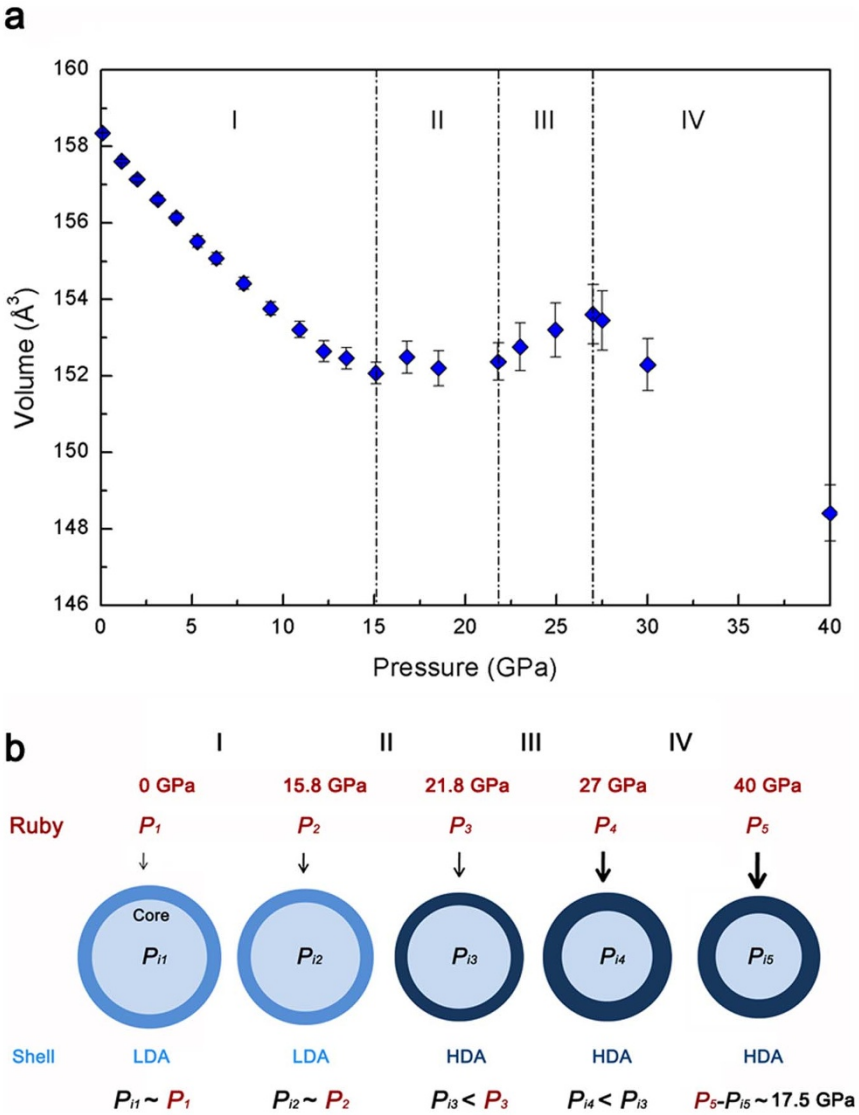

Figure 5 | (a) The pressure-dependent variations of the unit cell constants. (b) Compression mechanism in nc CeO_2 according to core-shell model, exaggerated for illustrative purposes. I: 0–15.1 GPa, isostress condition between low density amorphous (LDA) shell and crystalline core; II: 15.1–21.8 GPa, LDA → HDA transformations on the shell with compression; III: 21.8–27 GPa, negative volume compressibility region; IV: $P > 27$ GPa, the NVC phenomenon disappears owing to the yielding of the "hard" shell.

(ii) A larger fraction of the atoms belongs to the grain boundaries as the pressure elevated during compression[27],

we propose a mechanism here to explain the observed negative volume compressibility in 12 nm CeO_2 by extending the core-shell dual structure model. The initially LDA state will transform to a HDA state upon compression at a critical pressure. In other words, the surface shell get stiffer due to the LDA-HDA transformation under compression as compared to the nanocrystalline core[5]. Further compression, the core atoms near the interface transform to the amorphous state that belongs to the shell. At the same time, the residual core where XRD can detect relaxed due to the thicken of denser shell.

Schematic diagrams for the detailed structure evolution of the nanograin core-shell model under compression are shown in Fig. 5. The surface atoms exist in a form of LDA state upon initial compression, and the stress is continuous across the interface between LDA shell and crystalline core (so called isostress condition). The unit cell volume of nc CeO_2 decreases under compression at this stage (I: 0–15.1 GPa). A "hard" HDA shell[26] of the individual nanograin comes into being at stage II ($P \sim 15.1$–21.8 GPa). Due to the support of the "hard" amorphous shell (arching effect), the environment pressure is not timely delivered to the crystalline nanograin core, resulting in a pressure difference between the crystalline core and PTM. In other words, there exists pressure gradient from the HDA shell to the crystalline core ($P_{i2} < P_2$). Unlike isostress condition, the strain is continuous across the interface between HDA shell and crystalline core (isostrain condition) at stage II. Due to the epitaxial effect of

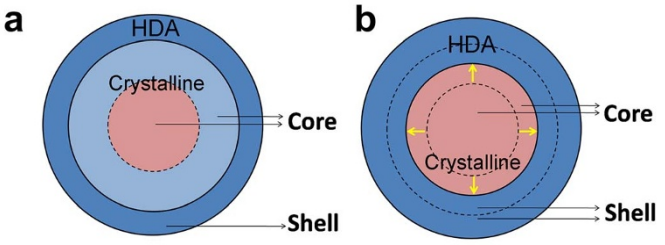

Figure 6 | **Negative volume compressibility region (III: 21.8–27 GPa).** (a) the light blue and red part: crystalline core; the blue part: HDA shell; (b) the blue part: HDA shell; the red part: residual crystalline core.

HDA at stage III ($P \sim 21.8$–27 GPa, Fig. 6), further compression can leads more crystalline core atoms, which are near to the shell-core interface, transform to the HDA shell atoms, which is a slow but continuous process[28]. Meanwhile, the residual crystalline core is relaxed owing to the thickening of HDA shell as the crystalline core has a lower density (longer Ce-O bonds) than that of the HDA shell (shorter Ce-O bonds). That means the increasing environmental P gradually thicken the HDA shell and lessen the volume of the crystalline core where the actual pressure is becoming smaller because of the core's relaxation. In this case, the pressure obtained by ruby R_1-luminescence line shift is the environmental pressure of the nanograins, and the pressure corresponding to the unit cell volume of cubic CeO_2 determined from *in situ* ADXD reflects the inner pressure of crystalline nanograin core. This created an illusion of (environmental) pressure induced unit cell volume expansion of nc CeO_2 at stage III (NVC region). The differential stress between inside and outside the HDA shell increased with compression. In conjunction with Fig. 5a, we may obtain that the maximal differential stress (p_c) which the HDA shell can support is about 17.5 GPa between the crystalline core and PTM. After that the "hard" HDA shell start to yield at ~30 GPa, the unit cell volume decreases with increasing pressure (IV: $P > 27$ GPa). However, the ADXD observed compression curve of 12 nm CeO_2 in stage IV drifts rightward rather than returns to normal as a result of the differential stress (~17.5 GPa).

According to the above discussion, the unusual NVC phenomenon observed in nc CeO_2 is attributed to the following two conditions: a) a stiff HDA shell can be formed under compression and the caused nano arching effect is strong enough to maintain an apparent stress difference between inside and outside of the shell; and b) part of the relative low density crystalline core atoms can transform to high density shell atoms, which can lower the actual core pressure.

For the first condition, it depends on the external environment and the intrinsic properties of the nanograin. With regard to the external environment, the degree of hydrostaticity plays an important role to maintain the HDA shell. When pressure acts on the core-shell structure, it is easier for the uniaxial pressure to break the shells due to the shear stress, whereas the shells could endure much higher hydrostatic pressure since the applying force is isotropic. As the grain core size is reduced a larger fraction of the atoms belongs to the grain boundaries, the pressure thicken the HDA shell under hydrostatic compression. However, under nonhydrostatic compression, the grain cores immediately experience the compression because the shells were smashed at lower pressure. On the other hand, when the shells were subjected to the hydrostatic compression, the thickening HDA shell was able to sustain higher pressure[26,27,29,30]. Therefore, as shown in Fig. 4, the pressure evolution of cell volume under nonhydrostatic compression exhibits unusual (work hardening) behavior immediately after the formation of the HDA shell at $P > 12$ GPa. However, the nonhydrostaticity in the chamber destroy the HDA shell upon further compression.

Nanoparticles have a tendency to strongly aggregate for the high surface-to-volume ratios. Using a soft PTM will not provide hydrostatic compression of all the particles and the intergrain contacts will lead anyway to strong shear stresses even if the medium is still hydrostatic[31]. It is well known that silicon oil is a poor PTM, being "quasihydrostatic" only up to 3 GPa[32]. In fact, the bad hydrostaticity character of silicon oil might be the reason why the NVC could be observed. Ideally, the PTM will be located between the grains, hindering the grains to touch each other, phenomenon that will provoke strong uniaxial strains, and transmit the pressure to the inner crystalline core. However, good PTM like helium or neon are too soft to hinder the grains to touch each other, which would have the same effect than no PTM. Therefore, the compressibility for experiments used M-E as PTM, both previous works and our experiment, are similar to that of no PTM.

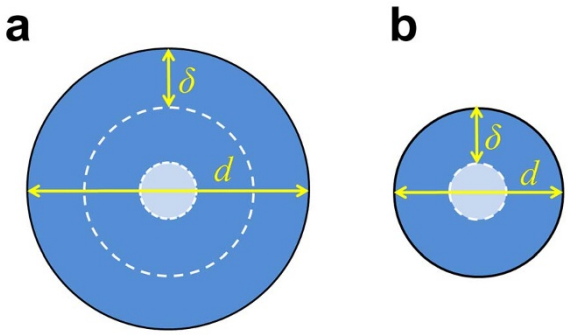

Figure 7 | Schematic diagrams for small grain size effect on abnormal compressibility. d is grain size and δ is the critical diameter for nucleation and growth of the HDA phase. (a) $d = 5\delta$. (b) $d = 3\delta$.

When it comes to the intrinsic properties of the nanograin, it depends on the strength and thickness of the shell, as well as the size of individual nanograin. After the formation of the hard amorphous shell, every grain can be viewed as a perfect spherical shell under uniform external pressure for simplicity's sake. For a perfect spherical shell, there are two possible failure modes (the HDA shell is yield or break). One is the maximum stresses reaching the yield condition and then yielding zone spread leading to final plastic collapse and the other is elastic or elastic-plastic buckling leading to collapse[33].

The maximum stress (p_c) supported by the hard HDA shell can be calculated by the following formula[34]:

$$p_c = k \cdot E \cdot \left(\frac{2r}{d}\right)^2, \qquad (1)$$

where

E = modulus of elasticity, GPa;
r = shell thickness, nm;
d = particle diameter, nm;
k = constant.

Here we make a qualitative discussion using the simplest type, therefore k is a certain coefficient without an exact value.

As reported in this work, p_c is about 17.5 GPa as the grain size is ~12 nm for CeO_2. The estimated maximum stress p_c for 12 μm CeO_2 is then ~0.18 bar, for the case where the HDA thickness r contribution has been neglected in equation (1). If it was to be included, then the maximum stress p_c may be far less than 0.18 bar. This demonstrates that p_c could be ignored as it is only 0.18 bar, which is comparable with the error brought by pressure standard. Let alone the fine crystallinity for micron materials on the surface which will hinder the shape up of HDA shell. Since the spherical shell is becoming a failure mode, the NVC phenomenon won't happen for 12 μm CeO_2.

The compression curve will be hardening after the formation of the stiff HDA shell that is strong enough to maintain an apparent stress difference between inside and outside of the shell for smaller grain size particle. However, whether NVC phenomenon will happen or not is depend on the second condition, since the initial nanocrystalline core should be larger than the critical nucleus as the size of any stable single crystal cannot be infinitely small. Fig. 7 illustrates this point. The critical diameter for nucleation and growth of the HDA phase is δ. When the grain diameter $d = 5\delta$ as shown in Fig. 7a, the lower compressibility occurs when the first shell formed and the NVC take place when the second shell comes into being; however, as shown in Fig. 7b ($d = 3\delta$), nothing but the lower compressibility occurs when the one and only first shell formed. This may be the reason why, without NVC phenomenon, only lower compressibility of 4.7 nm (5.6 nm) CeO_2 at $P > 10$ GPa (16 GPa) was observed in Ref. 5.

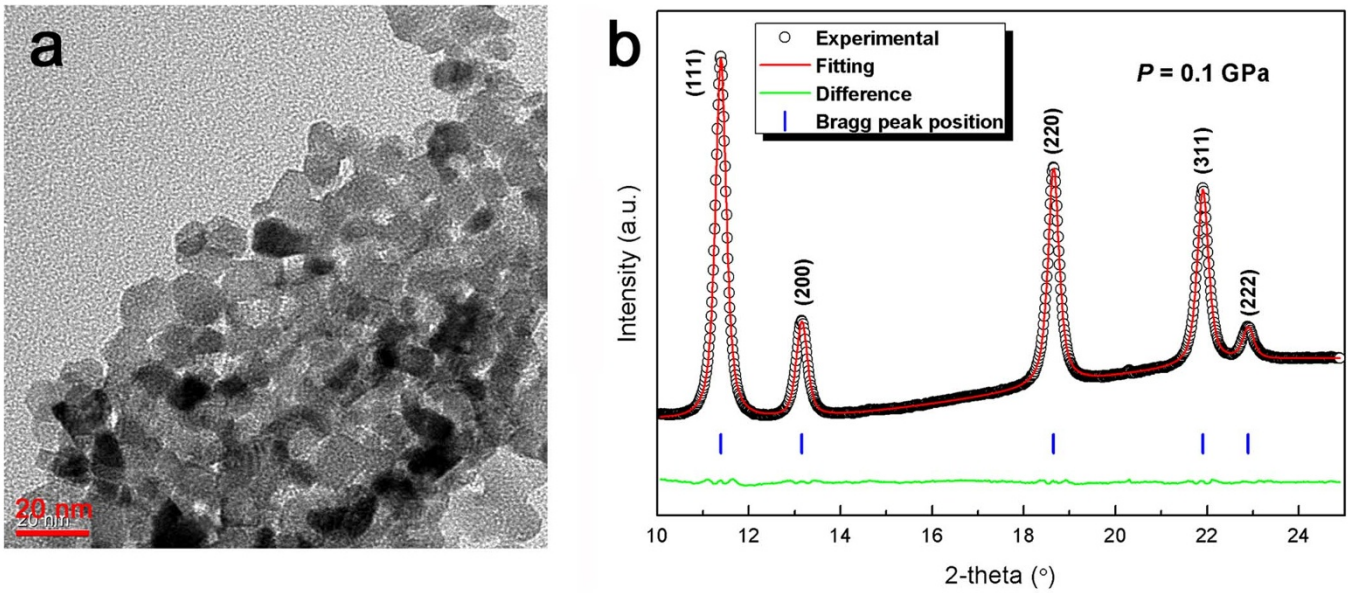

Figure 8 | (a) Transmission electron micrograph (TEM) of ~12 nm nc CeO_2. (b) An example of Rietveld refinement for nc CeO_2 under quasihydrostatic compression ($P = 0.1$ GPa, $a = 5.410129(74)$ Å, $V = 158.3517(65)$ Å^3).

Therefore, the NVC phenomenon may only be observed in nanomaterials with an average grain size around a critical dimension d_c. A potentially interesting subject for future high pressure studies of nanostructured materials is to check whether there is an indeed critical grain size d_c around which NVC would happen by a mechanism result from the dual structure model. On the other hand, the unusual structural stability and hardening of longitudinal modulus[9,35,36] for many nanostructured materials like nc CeO_2 under compression may also be rationalized by the hard-shell model mentioned above.

However, we present an analysis of such a structure under ideal conditions. Particle aggregation, dislocation activity in the grains, sliding motions at grain boundaries and increased nonhydrostaticity due to unavoidable solidification of liquid pressure media will hinder the shape up of, even break the HDA shell. Anyhow, this peculiar hard-shell structure is still suggested to be responsible for the observed increasing strength and toughness in some materials as the grain size decreases from micro to nano- scale.

In summary, we have identified the occurrence of "negative cell volume compressibility" in 12 nm CeO_2 via the use of *in situ* angle-dispersive synchrotron XRD. While the nanoscale CeO_2 has XRD characteristic of cubic fluorite phase up to ~40 GPa, the expansion of the unit cell causes a negative volume compressibility of the material under quasihydrostatic compression. This unusual behavior can be attributed to the formation and thicken of the stiff high density amorphous shell under compression, which causes a strong nano arching effect and lowers the actual crystalline core pressure for the individual nano grain.

Methods

Materials. The commercial nanocrystalline CeO_2 used in this study was purchased from Nanostructured & Ammorphous Materials Incorporated. The structure of the starting material was confirmed to be pure cubic fluorite phase ($Fm3m$) CeO_2 by ambient-pressure x-ray diffraction (XRD). The Scherrer formula has been used to deduce an average particle size of 12 nm from the (111), (200), (220), (311), (222), (400), (331), (420) and (422) diffraction linewidths, consistent with the value (12 ± 3 nm) of the dimension of the platelet grains discerned in the TEM micrograph of Fig. 8a.

DAC experiments. A modified Mao-Bell type DAC with a culet size of 300 μm was used to generate high pressures up to ~40 GPa. A piece of ~20-micron sample in thickness was loaded into a 100 μm diameter hole of a stainless steel (T301), which was preindented to 40 micron thickness. The thickness of squeezed sample powder at the highest pressure (~35 GPa) should be less than the gap between the diamond anvils. We conducted three separated experiments using the same starting material. In the first or second run, M-E (4 : 1) or silicone oil was used as a PTM and the internal pressure was measured using the ruby fluorescence lines[37]. In the third run, no PTM was used to achieve a maximum nonhydrostatic stress and a small amount of gold powder (<2%) was included to determine the pressure, using the equation of state of gold[38].

X-ray diffraction measurements. *In situ* high pressure angle dispersive diffraction experiments were performed at the High-Pressure Station, 4W2 beamline at Beijing Synchrotron Radiation Facility (BSRF). The x-ray was monochromatized to 0.6199 Å using double crystal (silicon 220). All of the measurements were conducted at room temperature. The two dimensional diffraction patterns were integrated by Fit2D[39] obtain the 2θ intensity curves, which were then analyzed by GSAS + EXPGUI Rietveld package[40,41] (Fig. S4) and PeakFit (Fig. 8b).

1. Zhai, T. *et al.* A Comprehensive Review of One-Dimensional Metal-Oxide Nanostructure Photodetectors. *Sensors* **9**, 6504–6529 (2009).
2. Kašpar, J., Fornasiero, P. & Graziani, M. Use of CeO_2-based oxides in the three-way catalysis. *Catal. Today* **50**, 285–298 (1999).
3. Wang, Z. L. & Feng, X. Polyhedral Shapes of CeO_2 Nanoparticles. *J. Phys. Chem. B* **107**, 13563–13566 (2003).
4. Kang, Z. & Wang, Z. L. Novel Oxides for Cycled Hydrogen Production from Methane and Water Using a Temperature Swing. *Adv. Mater.* **15**, 521–526 (2003).
5. Ge, M. Y. *et al.* Anomalous compressive behavior in CeO_2 nanocubes under high pressure. *New J. Phys.* **10**, 123016 (2008).
6. Duclos, S. J., Vohra, Y. K., Ruoff, A. L., Jayaraman, A. & Espinosa, G. P. High-pressure x-ray diffraction study of CeO_2 to 70 GPa and pressure-induced phase transformation from the fluorite structure. *Phys. Rev. B* **38**, 7755–7758 (1988).
7. Dogra, S. *et al.* High pressure behavior of nano-crystalline CeO_2 up to 35 GPa: a Raman investigation. *High Pressure Res.* **31**, 292–303 (2011).
8. Rekhi, S., Saxena, S. K. & Lazor, P. High-pressure Raman study on nanocrystalline CeO_2. *J. App. Phys.* **89**, 2968–2971 (2001).
9. Wang, Z., Saxena, S. K., Pischedda, V., Liermann, H. P. & Zha, C. S. In situ x-ray diffraction study of the pressure-induced phase transformation in nanocrystalline CeO_2. *Phys. Rev. B* **64**, 012102 (2001).
10. Wang, Z., Zhao, Y., Schiferl, D., Zha, C. S. & Downs, R. T. Pressure induced increase of particle size and resulting weakening of elastic stiffness of CeO_2 nanocrystals. *App. Phys. Lett.* **85**, 124–126 (2004).
11. Liu, B. *et al.* High-pressure Raman study on CeO_2 nanospheres self-assembled by 5 nm CeO_2 nanoparticles. *Phys. Status Solidi (B)* **248**, 1154–1157 (2011).
12. Liu, L. *et al.* Strength and equation of state of fluorite phase CeO_2 under high pressure. *J. App. Phys.* **112**, 013532–6 (2012).
13. Gerward, L. *et al.* Bulk modulus of CeO_2 and PrO_2-An experimental and theoretical study. *J. Alloy. Compd.* **400**, 56–61 (2005).
14. Liu, B. *et al.* Study of high pressure structural stability of CeO_2 nanoparticles. *Chinese Phys. C* **37**, 098003 (2013).
15. Chen, B. *et al.* Size-dependent elasticity of nanocrystalline titania. *Phys. Rev. B* **79**, 125406 (2009).

16. Liu, B. *et al.* High-Pressure Studies on CeO_2 Nano-Octahedrons with a (111)-Terminated Surface. *J. Phys. Chem. C* **115**, 4546–4551 (2011).
17. Kourouklis, G. A., Jayaraman, A. & Espinosa, G. P. High-pressure Raman study of CeO_2 to 35 GPa and pressure-induced phase transformation from the fluorite structure. *Phys. Rev. B* **37**, 4250–4253 (1988).
18. Birch, F. Finite strain isotherm and velocities for single-crystal and polycrystalline NaCl at high pressures and 300°K. *J. Geophys. Res.* **83**, 1257–1268 (1978).
19. Kornblatt, J. A. Materials with Negative Compressibilities. *Science* **281**, 143 (1998).
20. Lee, Y. *et al.* Non-framework cation migration and irreversible pressure-induced hydration in a zeolite. *Nature* **420**, 485–489 (2002).
21. Barnes, P. W., Woodward, P. M., Lee, Y., Vogt, T. & Hriljac, J. A. Pressure-Induced Cation Migration and Volume Expansion in the Defect Pyrochlores $ANbWO_6$ ($A = NH^{4+}$, Rb^+, H^+, K^+). *J. Am. Chem. Soc.* **125**, 4572–4579 (2003).
22. Fortes, A. D., Suard, E. & Knight, K. S. Negative Linear Compressibility and Massive Anisotropic Thermal Expansion in Methanol Monohydrate. *Science* **331**, 742–746 (2011).
23. Brazhkin, V. V., Katayama, Y., Kanzaki, M., Kondrin, M. V. & Lyapin, A. G. Pressure-induced structural transformations and the anomalous behavior of the viscosity in network chalcogenide and oxide melts. *JETP Lett.* **94**, 161–170 (2011).
24. Brazhkin, V. V. & Lyapin, A. G. High-pressure phase transformations in liquids and amorphous solids. *J. Phys.: Condens. Mat.* **15**, 6059 (2003).
25. Palosz, B. *et al.* High pressure x-ray diffraction studies on nanocrystalline materials. *J. Phys.: Condens. Mat.* **16**, S353 (2004).
26. Ma, Y. *et al.* High-pressure x-ray diffraction study of the giant dielectric constant material $CaCu_3Ti_4O_{12}$: Evidence of stiff grain surface. *Appl. Phys. Lett.* **88**, 191903–3 (2006).
27. Schiotz, J., Di Tolla, F. D. & Jacobsen, K. W. Softening of nanocrystalline metals at very small grain sizes. *Nature* **391**, 561–563 (1998).
28. Yip, S. Nanocrystals: The strongest size. *Nature* **391**, 532–533 (1998).
29. Palosz, B. *et al.* Analysis of short and long range atomic order in nanocrystalline diamonds with application of powder diffractometry. *Z. Kristallogr.* **217**, 497–509 (2002).
30. Fan, G. J., Choo, H., Liaw, P. K. & Lavernia, E. J. A model for the inverse Hall-Petch relation of nanocrystalline materials. *Mater. Sci. Eng. A* **409**, 243–248 (2005).
31. Machon, D. *et al.* Pressure-induced polyamorphism in TiO_2 nanoparticles. *Phys. Rev. B* **82**, 140102 (2010).
32. Brazhkin, V. V., Lyapin, A. G. & Trachenko, K. Atomistic modeling of multiple amorphous-amorphous transitions in SiO_2 and GeO_2 glasses at megabar pressures. *Phys. Rev. B* **83**, 132103 (2011).
33. Carlson, R. L., Sendelbeck, R. L. & Hoff, N. J. Experimental studies of the buckling of complete spherical shells. *Exp. Mech.* **7**, 281–288 (1967).
34. Pan, B. & Cui, W. An overview of buckling and ultimate strength of spherical pressure hull under external pressure. *Mar. Struct.* **23**, 227–240 (2010).
35. Jiang, J. Z., Olsen, J. S., Gerward, L. & Mørup, S. Enhanced bulk modulus and reduced transition pressure in γ-Fe_2O_3 nanocrystals. *Europhys. Lett.* **44**, 620 (1998).
36. Tolbert, S. H. & Alivisatos, A. P. High-Pressure Structural Transformations in Semiconductor Nanocrystals. *Annu. Rev. Phys. Chem.* **46**, 595–626 (1995).
37. Mao, H. K., Bell, P. M., Shaner, J. W. & Steinberg, D. J. Specific volume measurements of Cu, Mo, Pd, and Ag and calibration of the ruby R_1 fluorescence pressure gauge from 0.06 to 1 Mbar. *J. Appl. Phys.* **49**, 3276–3283 (1978).
38. Dewaele, A., Loubeyre, P. & Mezouar, M. Equations of state of six metals above 94 GPa. *Phys. Rev. B* **70**, 094112 (2004).
39. Hammersley, A. P., Svensson, S. O., Hanfland, M., Fitch, A. N. & Hausermann, D. Two-dimensional detector software: From real detector to idealised image or two-theta scan. *High Pressure Res.* **14**, 235–248 (1996).
40. Toby, B. EXPGUI, a graphical user interface for GSAS. *J. Appl. Crystallogr.* **34**, 210–213 (2001).
41. Verma, A. K., Ravindran, P., Rao, R. S., Godwal, B. K. & Jeanloz, R. On the stability of rhenium up to 1 TPa pressure against transition to thebcc structure. *B. Mater. Sci.* **26**, 183–187 (2003).

Acknowledgments

This work was performed at the Beijing Synchrotron Radiation Facility (BSRF, China), which is supported by Chinese Academy of Sciences under Grant No. KJCX2-SWN03 and No. KJCX2-SW-N20. The authors thank Lun Xiong, Chuanlong Lin, Rui Li, Xiaodong Li and Yanchun Li for experimental assistance. This work is supported by the China 973 Program (Grant No. 2011CB808200), National Natural Science Foundation of China (Grant No. 11027405), and National Natural Science Foundation of China-NSAF (Grant No. 10976018).

Author contributions

Q.M.W. and D.W.H. was involved in the study design and the drafting of the manuscript, performed most of the experiments and performed data analysis. F.P. and L.L. conducted DAC experiments. P.P.L., S.Y., P.W. and C.X. conducted synchrotron x-ray experiments at high pressures. J.L. was responsible for the beamline 4W2 of the Beijing Synchrotron Radiation Facility. All authors reviewed the manuscript.

Additional information

Supplementary information accompanies this paper at http://www.nature.com/scientificreports

Competing financial interests: The authors declare no competing financial interests.

How to cite this article: Wang, Q.M. *et al.* Unusual Compression Behavior of Nanocrystalline CeO_2. *Sci. Rep.* **4**, 4441; DOI:10.1038/srep04441 (2014).